Int J Earth Sci (Geol Rundsch) (2017) 106:1123–1131
DOI 10.1007/s00531-016-1361-9

ORIGINAL PAPER

Three-dimensional imaging of the S-velocity structure for the crust and the upper mantle beneath the Arabian Sea from Rayleigh wave analysis

V. Corchete[1]

Received: 24 February 2016 / Accepted: 25 June 2016 / Published online: 9 July 2016
© Springer-Verlag Berlin Heidelberg 2016

Abstract A 3D imaging of S-velocity for the Arabian Sea crust and upper mantle structure is presented in this paper, determined by means of Rayleigh wave analysis, for depths ranging from zero to 300 km. The crust and upper mantle structure of this region of the earth never has been the subject of a surface wave tomography survey. The Moho map performed in the present study is a new result, in which a crustal thickening beneath the Arabian Fan sediments can be observed. This crustal thickening can be interpreted as a quasi-continental oceanic transitional structure. A crustal thickness of up to 20 km also can be observed for the Murray Ridge system in this Moho map. This crustal thickening can be due to that the Murray Ridge System consists of Indian continental crust. This continental crust is extremely thinned to the southwest of this region, as shown in this Moho map. This area can be interpreted as oceanic in origin. In the depth range from 30 to 60 km, the S-velocity presents its lower values at the Carlsberg Ridge region, because it is the younger region of the study area. In the depth range from 60 to 105 km of depth, the S-velocity pattern is very similar to that shown for the previous depth range, except for the regions in which the asthenosphere is reached, for these regions appear a low S-velocity pattern. The lithosphere–asthenosphere boundary (LAB), or equivalently the lithosphere thickness, determined in the present study is also a new result, in which the lithosphere thickness for the Arabian Fan can be estimated in 60–70 km. The lower lithospheric thickness observed in the LAB map, for the Arabian Fan, shows that this region may be in the transition zone between continental and oceanic structure. Finally, a low-velocity zone (LVZ) has been determined, for the whole study area, located between the LAB and the boundary of the asthenosphere base (or equivalently the lithosphere–asthenosphere system thickness). The asthenosphere-base map calculated in the present study is also a new result.

Keywords Rayleigh wave · Shear wave · Crust · Upper mantle · Arabian Sea

Introduction

In comparison with other oceans and seas, very few geophysical studies have been made for the Arabian Sea. For it, any new geophysical study of this area is of interest to discover the material condition existing in its different parts. As the surface wave dispersion (Rayleigh wave dispersion) is very sensitive to the Earth's structure crossed by the waves, a Rayleigh wave dispersion analysis is a useful tool to reveal the features of the elastic structure beneath the Arabian Sea (represented by its 3D imaging of the S-velocity structure). The S-velocity structure obtained from this analysis, beneath the different geological environments of this area, can give important constraints for later geophysical and geological studies developed in this region and the surrounding areas. For instance, knowledge of the crustal velocity structure beneath the Arabian Sea can help in constructing an appropriate model for the evolution of the Indian Ocean.

In previous studies developed for the Arabian Sea region, Singh (1988, 1990) obtained some group velocity and attenuation curves from 10 to 100 s of period (for

Electronic supplementary material The online version of this article (doi:10.1007/s00531-016-1361-9) contains supplementary material, which is available to authorized users.

✉ V. Corchete
corchete@ual.es

[1] Higher Polytechnic School, University of Almeria, 04120 Almería, Spain

both Love and Rayleigh waves). He performs a unique S-velocity model (and P-velocity model), calculated from the dispersion curves, and some Q_β models computed from the attenuation curves. Later, Singh (1999) and Mitra et al. (2006) investigated the crust and upper mantle structure beneath the Indian subcontinent, using surface waves. In these studies, the Arabian Sea region is scarcely sampled. In other global studies, Montagner and Jobert (1988) and Debayle et al. (2001) performed seismic tomography for the Indian Ocean and the surroundings areas. In these studies, the Arabian Sea region is only a small part of the whole study area considered. As a result, this region is also scarcely sampled. On the other hand, in other small-scale studies, as the seismic and magnetic imaging performed by Gaedicke et al. (2002), the study area is considered as the Indus Fan, i.e., only a small part of the Arabian Sea region is considered under study. Thus, it should be noted that no detailed 3D S-velocity structure has been obtained for the Arabian Sea region. The S-velocity structure performed in the above-mentioned previous studies shows lack of resolution for this region. Also, it should be noted that the Arabian Sea crust and upper mantle structure never has been the subject of a surface wave tomography survey to achieve an appropriate 3D S-velocity model for this region.

Therefore, the goal of the present study is the determination of the elastic structure (S-velocity structure) beneath the Arabian Sea region, from Rayleigh wave analysis, for the whole depth range from 0 to 300 km. The period range to be obtained in the present study, by digital filtering, will be wider than the period range measured in the above-mentioned previous studies. Thus, the determination of the 3D S-velocity structure will be more accurate in the present study than in any other above-mentioned previous study.

Data set

In this study, a list of 122 earthquakes which occurred from 1989 to 2014 in the neighbouring of the study area, have been considered (Supplement 1). These earthquakes have been registered by 21 seismic stations located at this region (Supplement 2). From these stations, digital data are available, recorded with a different instrument for each available channel (Supplement 3), but only the most suitable data for this study have been considered (Corchete 2013), from all these available channels.

Methodology

For the Rayleigh wave analysis, the computation method detailed by Corchete (2013) and revised and improved by Corchete (2014) was followed. In this paper, only a brief review of this methodology will be presented.

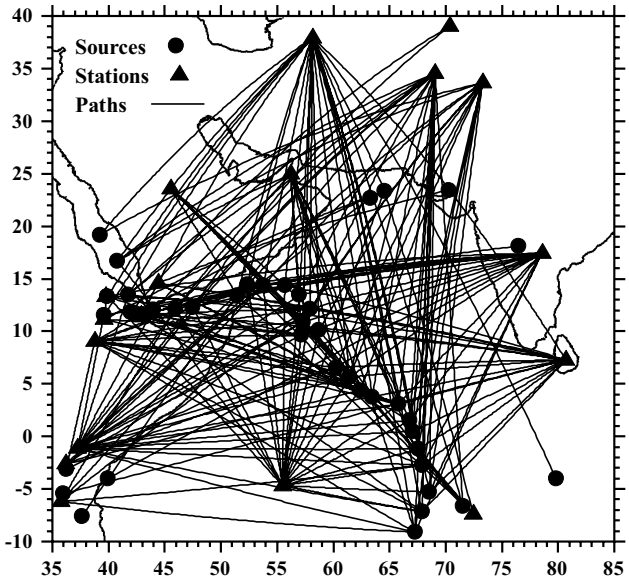

Fig. 1 Path coverage of the Rayleigh waves (212 paths)

Grouping of stations and seismic events

All the seismic events listed in Supplement 1 have been grouped in source zones, as listed in Supplement 4, to get source-station paths from epicentre-station paths. It should be noted that some stations considered in this study (Supplement 2) also show very similar coordinates. Thus, they have been also grouped defining new station codes to denote these average stations (Supplement 5). Figure 1 (and Supplement 6) shows the path coverage obtained for the study area (given by the source-station paths).

Dispersion analysis

The Rayleigh wave group velocity for the trace of each event registered has been measured by means of the combination of digital filtering techniques: multiple filter technique (Dziewonski et al. 1969) and time-variable filtering (Cara 1973), as shown in the flow chart displayed in Supplement 7 (Corchete et al. 2007). As an example of this filtering process, the application of this combination of filtering techniques to the trace of the event 35 (recorded at station ABKT) is presented in the Supplements 8, 9 and 10.

Average dispersion curves and estimation of the error

The average group velocities obtained for the 212 source-station paths considered in this study are listed in

Supplement 11 for several periods (period range from 5 to 175 s).

Regionalization of group velocities

Supplement 12 shows the regionalized group velocity $U(x, y)$, calculated from the above-mentioned data set, following the regionalization method detailed by Corchete (2014). Supplement 13 shows the errors $\Delta U(x, y)$ arisen in computation of the regionalized group velocity $U(x, y)$ shown in Supplement 12.

Inversion of regionalized dispersion curves

The regionalized group velocity surfaces $U(x, y)$ calculated for each period, from 5 to 175 s, are sampled in a rectangular grid of 40 × 40 points. Really, these grid points are the centres of a grid with 40 × 40 rectangular blocks, as the block shown in Supplement 14. These grid data can be inverted obtaining a shear velocity model (a shear velocity distribution with depth) for each grid point (or block) of the study area, achieving thus a 3D S-velocity model that represents the 3D elastic structure beneath the study area. In all cases, the water depth has been taken into account in the inversion procedure, because it has a substantial influence on the results at shallower depths. As an example of this inversion process, Supplement 16 shows the obtained results for the inversion of the dispersion curve corresponding to the block area shown in Supplement 14. The initial model considered in this example is listed in Supplement 15. For depths deeper than 300 km, the PREM model developed by Dziewonski and Anderson (1981) has been used. It should be noted that the S-velocity models (Supplement 16a) and the resolving kernels (Supplement 16b) are plotted only for depths above 800 km. This fact is due to the bad resolution obtained for depths deeper than 300 km (Supplement 16b). Therefore, the results obtained for depths below 300 km have been left out, because the resolution at these deeper depths is poor.

Shear velocity mapping

The above-described S-velocity distributions with depth, obtained for each grid point (or rectangular block) of the above-mentioned grid defined in the study area, are now plotted in contour maps. The 2D images of shear velocity for the study area are shown in Fig. 2 (and Supplement 17). The 1-sigma errors in the S-wave velocities are also represented by 2D images in Supplement 18, to check the error spatial distribution of the S-wave velocities mapped in Fig. 2.

Mapping of the principal discontinuities

The principal discontinuities in depth of the study area (Moho, lithosphere–asthenosphere boundary and asthenosphere base) have been mapped as shown in Fig. 3. These surfaces have been obtained from the 3D S-velocity structure determined in the present study (Fig. 2). The Moho map shown in Fig. 3 (top) has been performed considering that the S-velocity values higher than 4.0 km/s can be attributed to the mantle structure. Then, considering for each point of the study area the depth in which the S-velocity value jumps above 4 km/s, it is possible to define a surface that can be considered as the Moho boundary. The map of the lithosphere–asthenosphere boundary (or equivalently the lithosphere thickness), shown in Fig. 3 (middle), has been computed considering the depth in which the S-velocity starts to decrease with depth, below the Moho discontinuity. The asthenosphere-base map, shown in Fig. 3 (bottom), has been computed considering the depth in which the S-velocity starts to increase with depth below the LAB. The uncertainties in the computation of these surfaces increase with depth, because the layer thickness considered in the S-velocity models (Supplement 16) must be increased with depth, to get a better resolution (Corchete et al. 2007). Thus, an error of 2.km is estimated for depths ranging from 0 to 30 km, an error of 7 km for depths ranging from 30 to 80 km and an error of 12 km for depths ranging from 80 to 300 km.

Results and discussion

The obtained results in this study as shown in the S-velocity mapping of Fig. 2 will be presented and discussed. The structural features shown by these images will be also correlated with other geophysical studies (developed in the study area) and correlated with the geology.

Depth range: 0–10 km

The lower S-velocity values are correlated with the location of the thicker sedimentary basins (areas with a sediment thickness greater than 5 km). On the other hand, the higher S-velocity values are associated with the areas in which the crust is thinner (as the Carlsberg Ridge). In the Arabian Fan, lower values of group velocities, at the period range from 5 to 20 s, were observed by Singh (1999) and Mitra et al. (2006), due to the thick sedimentary deposits present in this area. The Arabian Fan is considered by Singh (1988) as the region of the Arabian Sea bounded by the Chagos–Laccadive Ridge in the east, by the Owen–Murray Ridges in the west and by the Carlsberg Ridge in the south (Fig. 4).

This region is called by Prins et al. (2000) as the Indus Fan. Nevertheless, Gaedicke et al. (2002) considered the Indus Fan as a smaller area located at the north of the Arabian Sea (Fig. 4). In this paper, the Arabian Fan will be considered as defined by Singh (1988, 1990) and the Indus fan as defined by Gaedicke et al. (2002). For the Indus Fan, it should be noted that S-velocity values are lower in areas with thicker sedimentary deposits and the S-velocity values increase when the sediment thickness decreases (Gaedicke et al. 2002).

Depth range: 10–30 km

The higher S-velocity values are now associated with the areas in which the Moho depth is overcome (i.e. zones in which the depth range considered is located below

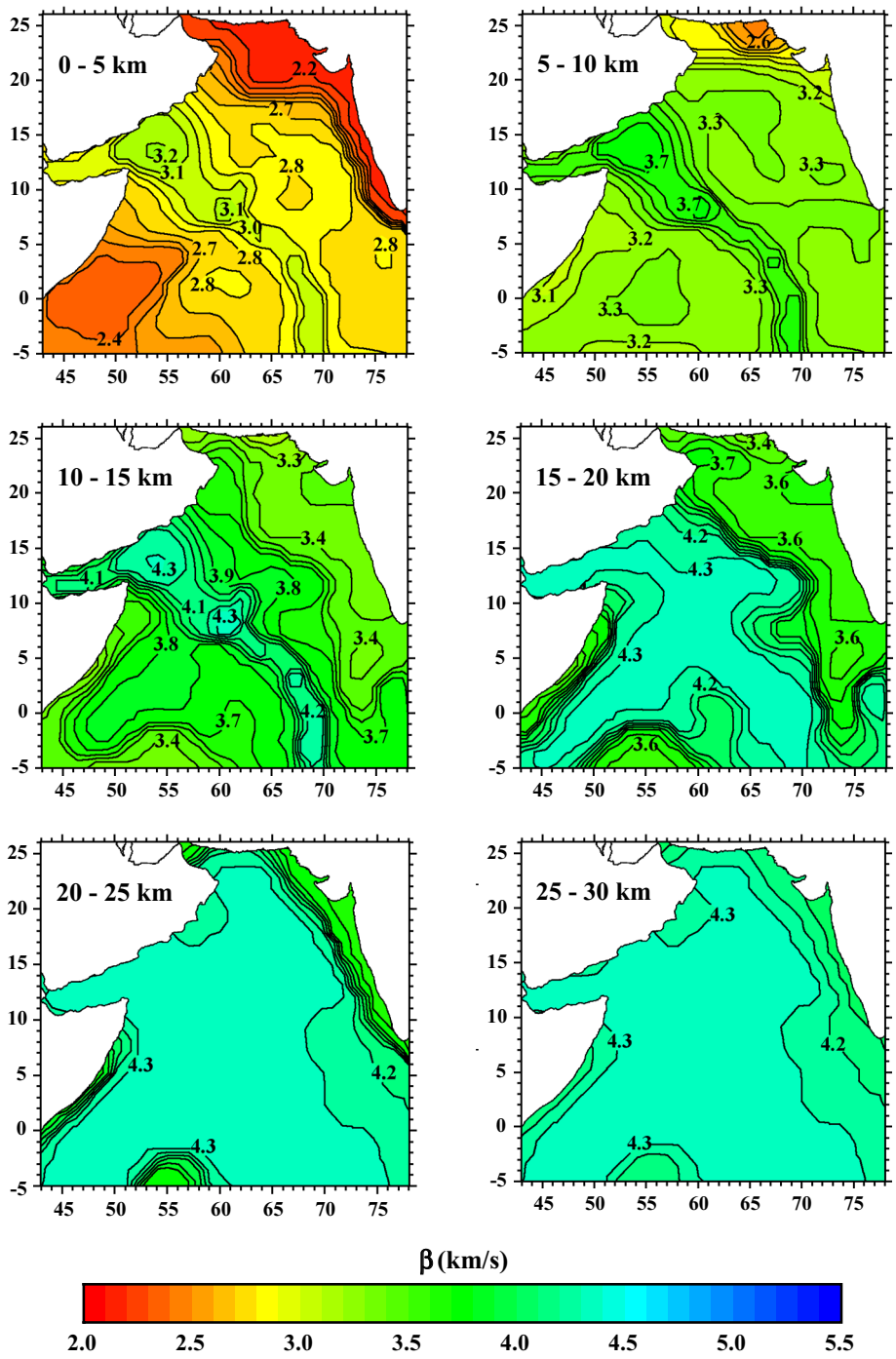

Fig. 2 Geographical distribution of the S-velocity, as a function of depth, plotted for the big rectangle shown in Supplement 14. The interval between isolines is 0.1 km/s

Fig. 2 continued

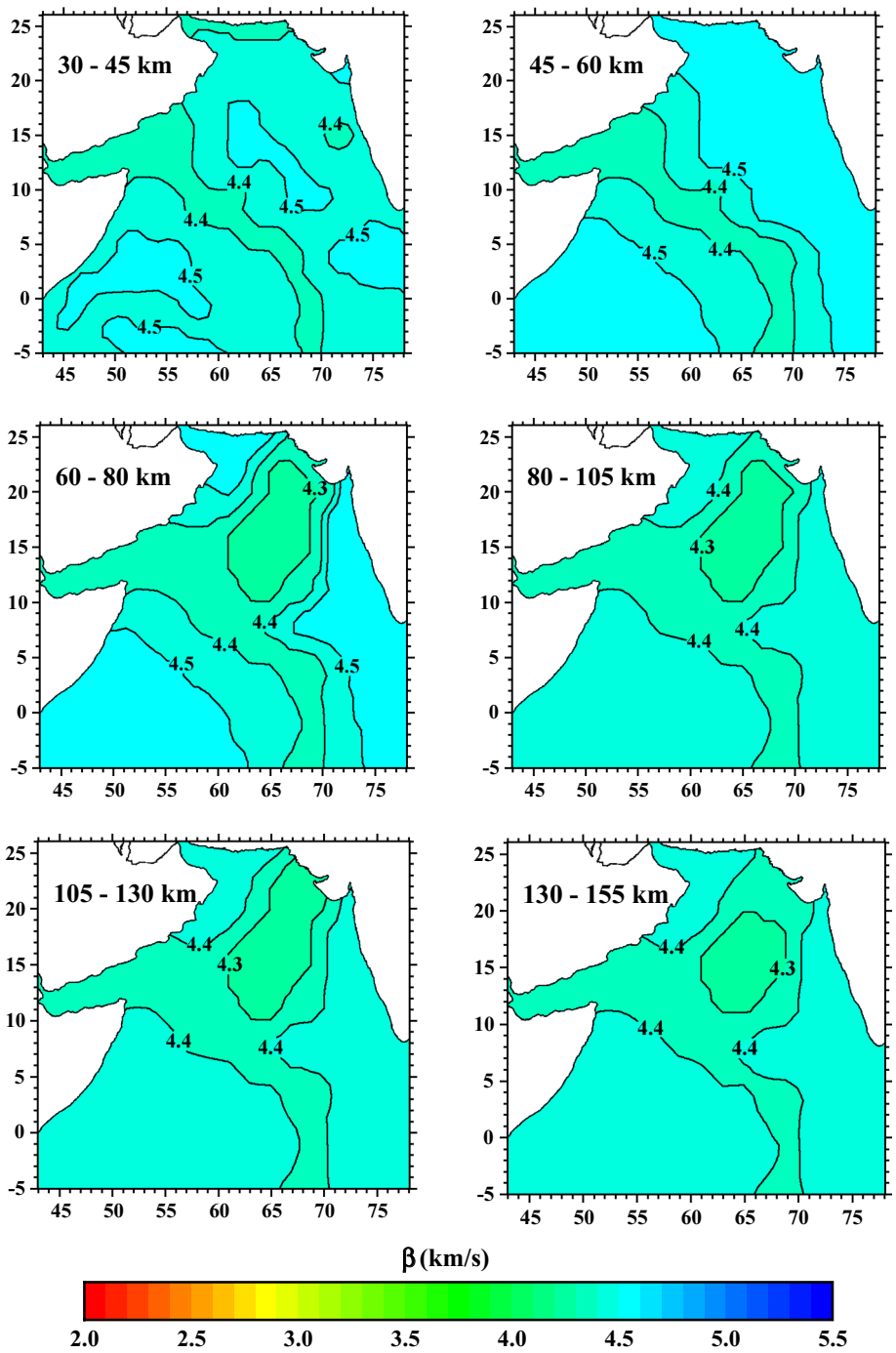

the Moho discontinuity). For each depth range shown in Fig. 2 (between 10 and 30 km), the Moho depth is overcome in different areas. In these areas, the S-velocity values higher than 4.0 km/s could be attributed to the mantle structure below the Moho discontinuity. This discontinuity is mapped in Fig. 3 (top). This new interesting Moho map is in good agreement with other previous studies. Singh (1988) found a crustal thickening beneath the Arabian Fan sediments which is in agreement with the Moho depth calculated in the present study (Fig. 3). He interpreted this crustal thickening as a quasi-continental oceanic transitional structure, i.e. as a quasi-continental oceanic structure transition from continent to ocean. From gravity modelling, Gaedicke et al. (2002) found evidence of a crustal thickness of up to 20 km, for the Murray Ridge system. In the present study, the Moho depth in the same area is found to be also 20 km (approximately). They supposed that the Murray Ridge System consists of Indian continental crust with magmatic components of different ages (Gaedicke et al. 2002). This continental crust is extremely thinned to

Fig. 2 continued

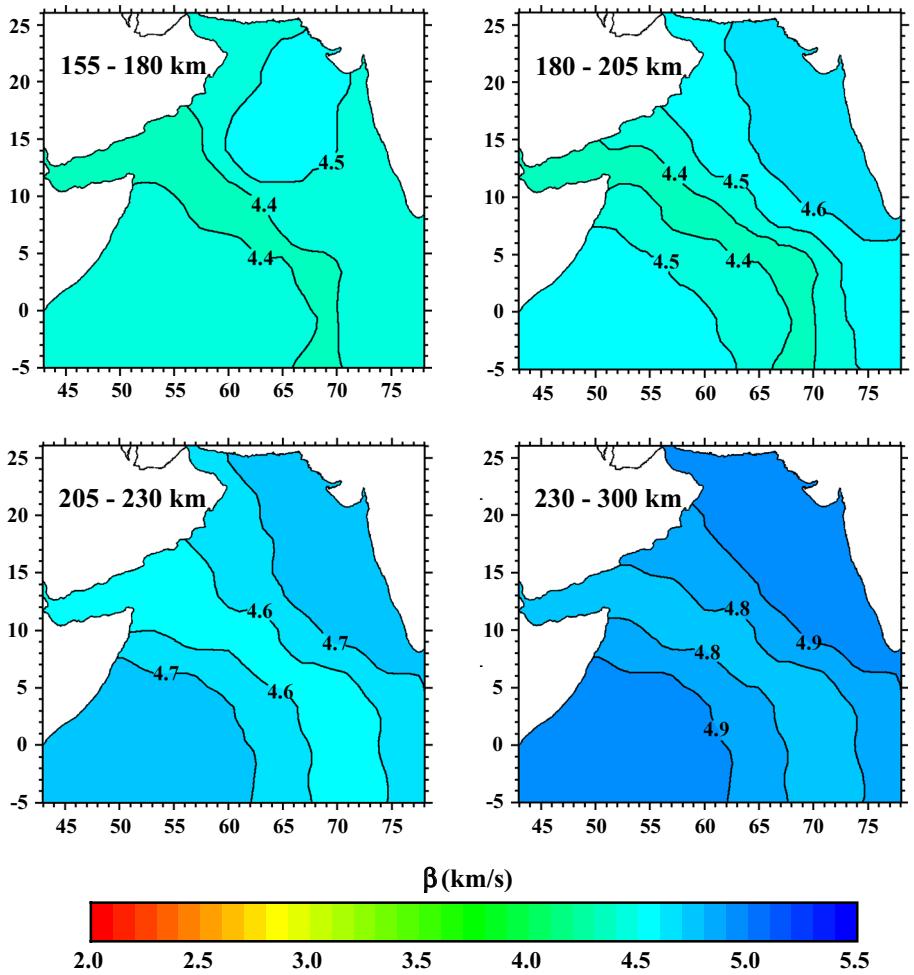

the southwest. Malod et al. (1997) previously interpreted this area as oceanic in origin. In the present study, also is observed a decrease in the Moho depth shown in Fig. 3 (top), for the southwest of the Murray Ridge region.

Depth range: 30–60 km

The S-velocity presents now its lower values at the younger regions of the study area, as the Carlsberg Ridge. The major part of the Arabian Sea was created by seafloor spreading along the Carlsberg Ridge (Chaubey et al. 1995). This S-velocity pattern supports the well-known hypothesis which states that the younger areas of the earth present lower S-velocity values than other older and more consolidate areas (e.g. Canas and Mitchell 1978, 1981).

Depth range: 60–80 km

The S-velocity pattern is very similar to that shown for the previous depth range, except for the regions in which the asthenosphere is reached, as shown in Fig. 3 (middle), for these regions appear a pattern of low S-velocity. The map of the lithosphere–asthenosphere boundary (LAB), shown in Fig. 3 (middle), is a new and very interesting feature determined in this study. Singh (1999) estimated the lithosphere thickness to be 70 km for the Arabian Fan, which is in agreement with this LAB map. He affirmed that the low lithospheric thickness in the Arabian Fan shows that the region may be in the transition zone between continental and oceanic structure. He also determined a zone of high attenuation (and high temperature) in the Arabian Fan below 60 km of depth, which coincides with the low S-velocity values shown in Fig. 2, at this depth and for this same region. Quittmeyer and Kafka (1984) suggested the subduction of the Arabian plate beneath the southern coast of Pakistan, as the cause of this increment of temperature.

Depth range: 80–155 km

The S-velocity shows the lowest values determined for the upper mantle, because the present depth range is below the LAB, for the whole study area, as shown in Fig. 3 (middle). Thus, a low-velocity zone (LVZ) exists, for the whole study area, located between the LAB and the boundary of

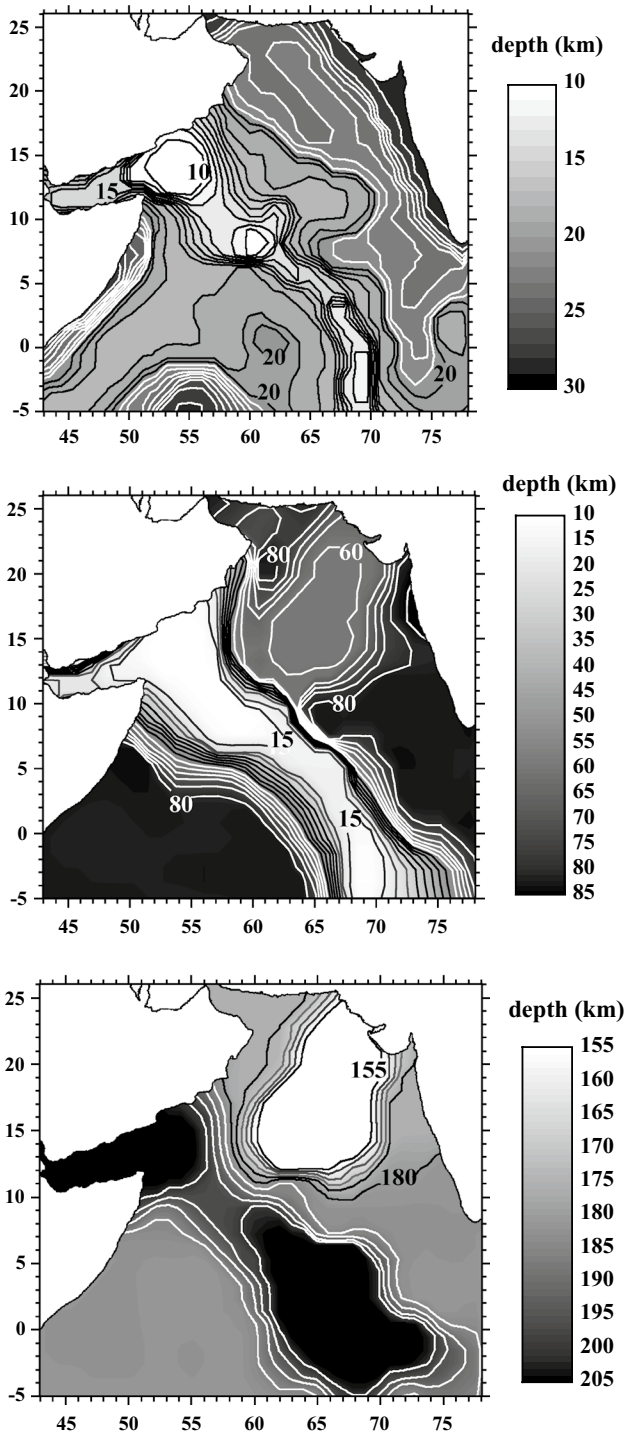

Fig. 3 Map of the Moho depth (*top*), the lithospheric thickness (*middle*) and the base of the asthenosphere (*bottom*); obtained from the 3D S-velocity structure shown in the 2D S-velocity mapping of Fig. 2. The interval between isolines is 1 km for the Moho map and 5 km for the plots of the lithosphere–asthenosphere boundary and the base of the asthenosphere

the asthenosphere base (or equivalently the lithosphere–asthenosphere system thickness) shown in Fig. 3 (bottom). The map of the asthenosphere base is also a new and very interesting feature determined in this study. For the Arabian Fan, the presence of this LVZ was previously reported by Singh (1988), who estimated a 100-km-thick LVZ at 64 km depth from the water surface, using surface wave dispersion data. Later, Singh (1990) found for the same region a high-attenuation zone at a depth of 60–160 km from the water surface, using Q_β models. The high-attenuation zone and the LVZ found by Singh (1988, 1990) agree well with the LVZ determined in the present study, as shown in Fig. 3 (middle and bottom). In other global seismic tomography (Montagner and Jobert 1988; Debayle et al. 2001) have been found slow S-velocity anomalies, deeper than 120 km of depth, below the Arabian Sea, which confirms the above-mentioned LVZ. Unfortunately, the Arabian Sea region is only a small part of the whole study area considered in these studies. For it, the resolution achieved in these studies for this region is generally a bad resolution, which makes difficult the comparison with the results achieved in the present study.

Depth range: 155–205 km

The S-velocity pattern is very similar to that shown for the previous depth range, except for the regions in which the asthenosphere is overcome, as shown in Fig. 3 (bottom), for these regions appear a pattern of high S-velocity.

Depth range: 205–300 km

The S-velocity values jump with respect to those shown in the previous depth ranges, reaching the highest values. Nevertheless, the S-velocity presents lower values at the younger regions of the study area, as the Carlsberg Ridge. This S-velocity pattern is the expected, because the younger areas of the earth generally present lower S-velocity values than other older and more consolidate areas. In other global seismic tomography (Montagner and Jobert 1988; Debayle et al. 2001), a similar S-velocity pattern is found, at this depth range, for the Arabian Sea region, but the bad resolution achieved in these mappings for this region makes difficult a detailed comparison with the results achieved in the present study.

Conclusions

In the depth range from 0 to 10 km, the lower S-velocity values correlate well with the location of the thicker sedimentary basins (areas with a sediment thickness greater than 5 km). For the Indus Fan, the S-velocity values increase when the sediment thickness decreases. At this depth range, the higher S-velocity values are associated with thinner crust (as the Carlsberg Ridge). For the depth

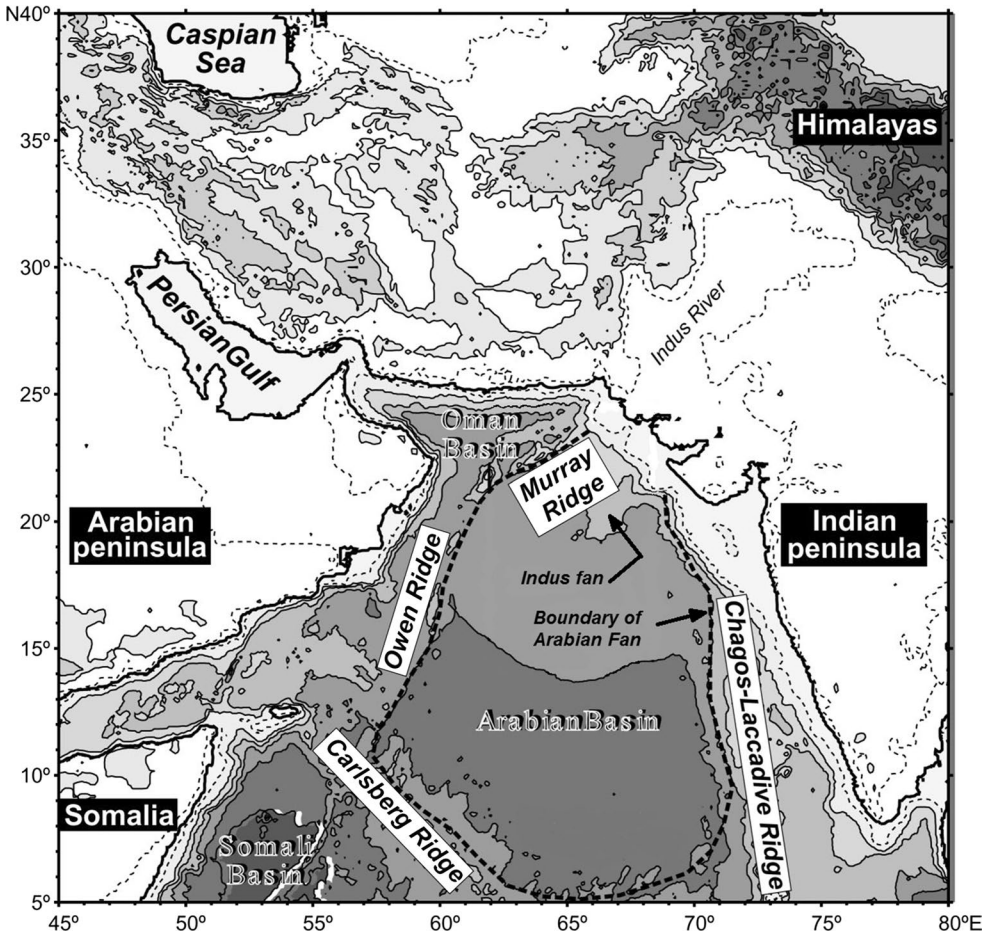

Fig. 4 Topography and bathymetry of the Arabian Sea and its surrounding land masses at a 1000-m contour interval, *dashed contour lines* are 2125 and 1200 m (Prins et al. 2000)

range from 10 to 30 km, the higher S-velocity values are associated with the Moho depth overcome (i.e. zones in which the depth range considered is located below the Moho discontinuity). The Moho map performed in the present study is a new and very interesting result, in which a crustal thickening beneath the Arabian Fan sediments can be observed. This crustal thickening can be interpreted as a quasi-continental oceanic transitional structure. A crustal thickness of up to 20 km also can be observed for the Murray Ridge system, in the obtained Moho map. This crustal thickening is attributed to the Murray Ridge System, which consists of Indian continental crust. On the other hand, this continental crust is extremely thinned to the southwest of this region. This area can be interpreted as oceanic in origin. In the depth range from 30 to 60 km, the S-velocity presents its lower values at the Carlsberg Ridge region, because it is the younger region of the study area, as the major part of the Arabian Sea was created by seafloor spreading along this region. In the depth range from 60 to 105 km, the S-velocity pattern is very similar to that shown for the previous depth range, except for the regions in which the asthenosphere is reached, showing a low S-velocity pattern for these regions. The lithosphere–asthenosphere boundary (or equivalently the lithosphere thickness) determined in the present study is also a new and very interesting result, in which the lithosphere thickness for the Arabian Fan is estimated at 60–70 km. The lower lithospheric thickness observed in the LAB map, for the Arabian Fan, shows that this region may be in the transition zone between continental and oceanic structure. Finally, a low-velocity zone (LVZ), for the whole study area, is located between the LAB and the boundary of the asthenosphere base (or equivalently the lithosphere–asthenosphere system thickness). The calculated asthenosphere-base map is also a new and very interesting result.

Acknowledgements The author is grateful to the National Geophysical Data Center (NGDC) and the Incorporated Research Institutions for Seismology (IRIS), for providing data used in this study. The elevation data have been retrieved from NGDC, through the database ETOPO1 (available by HTTP internet protocol). The seismograms and the instrumental response have been retrieved from IRIS (through the Internet utility WILBER 3) and from the database IRIS DMC MetaData Aggregator (available by HTTP internet protocol), respectively.

References

Canas JA, Mitchell BJ (1978) Lateral variation of surface anelastic attenuation across the Pacific. Bull Seismol Soc Am 68:1637–1650

Canas JA, Mitchell BJ (1981) Rayleigh wave attenuation and its variation across the Atlantic Ocean. Geophys J R Astron Soc 67:159–176

Cara M (1973) Filtering dispersed wavetrains. Geophys J R Astron Soc 33:65–80

Chaubey AK, Bhattacharya GC, Gopala Rao D (1995) Seafloor spreading magnetic anomalies in the southeastern Arabian Sea. Mar Geol 128:105–114

Corchete V (2013) Shear-wave velocity structure of Antarctica from Rayleigh-wave analysis. Tectonophysics 583:1–15

Corchete V (2014) Shear-wave velocity structure of Australia from Rayleigh-wave analysis. Earth Sci Res J 18:87–98

Corchete V, Chourak M, Hussein HM (2007) Shear wave velocity structure of the Sinai Peninsula from Rayleigh wave analysis. Surv Geophys 28:299–324

Debayle E, Lévêque J-J, Cara M (2001) Seismic evidence for a deeply rooted low-velocity anomaly in the upper mantle beneath the northeastern Afro/Arabian continent. Earth Planet Sci Lett 193:423–436

Dziewonski AM, Anderson DL (1981) Preliminary reference earth model. Phys Earth Planet Inter 25:297–356

Dziewonski A, Bloch S, Landisman M (1969) A technique for the analysis of transient seismic signals. Bull Seismol Soc Am 59:427–444

Gaedicke C, Schlüter H-U, Roeser HA, Prexl A, Schreckenberger B, Meyer H, Reichert C, Clift P, Amjad S (2002) Origin of the northern Indus Fan and Murray Ridge, Northern Arabian Sea: interpretation from seismic and magnetic imaging. Tectonophysics 355:127–143

Malod JA, Droz L, Mustafa Kemal B, Patriat P (1997) Early spreading and continental to oceanic basement transition beneath the Indus deep-sea fan. Mar Geol 141(1/4):221–235

Mitra S, Priestley K, Gaur VK, Rai SS, Haines J (2006) Variation of Rayleigh wave group velocity dispersion and seismic heterogeneity of the Indian crust and uppermost mantle. Geophys J Int 164:88–98

Montagner J-P, Jobert N (1988) Vectorial tomography—II. Application to the Indian Ocean. Geophys J Int 94:309–344

Prins MA, Postma G, Cleveringa J, Cramp A, Kenyon NH (2000) Controls on terrigenous sediment supply to the Arabian Sea during the late Quaternary: the Indus Fan. Mar Geol 169:327–349

Quittmeyer RC, Kafka AL (1984) Constraint on plate motions in southern Pakistan and northern Arabian Sea from the focal mechanism of small earthquakes. J Geophys Res 89:2444–2458

Singh DD (1988) Quasicontinental-oceanic structure beneath the Arabian Fan sediments from the observed surface wave dispersion studies. Bull Seismol Soc Am 78:1510–1521

Singh DD (1990) Q-structure beneath the north and central Indian Ocean from the inversion of observed Love and Rayleigh wave attenuation data. Phys Earth Planet Inter 59:243–258

Singh DD (1999) Surface wave tomography studies beneath the Indian subcontinent. J Geodyn 28:291–301